Atmospheric Moisture Decreases Mid-Latitude Eddy Kinetic Energy

Nicholas Lutsko[1], Nicholas J Lutsko[2], José Martinez-Claros[2], and Daniel D B Koll[3]

[1]Affiliation not available
[2]Scripps Institution of Oceanography, University of California at San Diego
[3]Laboratory for Climate and Ocean-Atmosphere Studies, Dept. of Atmospheric and Oceanic Sciences, Peking University

December 27, 2023

Atmospheric Moisture Decreases Mid-Latitude Eddy Kinetic Energy

Nicholas J. Lutsko[a] , José Martinez-Claros[a] , Daniel D. B. Koll[b]

[a] *Scripps Institution of Oceanography, University of California at San Diego, La Jolla, CA, USA*

, [b] *Laboratory for Climate and Ocean-Atmosphere Studies, Dept. of Atmospheric and Oceanic Sciences, Peking University, Beijing, China*

Corresponding author: Nicholas Lutsko, nlutsko@ucsd.edu

ABSTRACT: There is compelling evidence that atmospheric moisture may either increase or decrease mid-latitude eddy kinetic energy (EKE). We reconcile these pieces of evidence by using a hierarchy of idealized atmospheric models to demonstrate that moisture energizes individual eddies, but makes the large-scale conditions in which they form less favorable for eddy growth. For Earth-like climates, the latter effect wins out, and moisture weakens mid-latitude eddy activity. The model hierarchy includes a moist two-layer quasi-geostrophic (QG) model and an idealized moist general circulation model (GCM). In the QG model, EKE increases when moisture is added to simulations with fixed baroclinicity, closely following a previously derived scaling. But in both models moisture decreases EKE when environmental conditions are allowed to vary, though for different reasons. We explain these results by examining the models' Mean Available Potential Energy (MAPE) and by calculating terms in the Lorenz Energy Cycle. Finally, we discuss the connection between these results and related studies of the atmosphere's entropy budget and atmospheric work. Together, these results clarify moisture's role in driving the mid-latitude circulation and also highlight several drawbacks of QG models for studying moist processes.

SIGNIFICANCE STATEMENT: Dry models of the atmosphere have played a central role in the study of large-scale atmospheric dynamics. But we know that moisture adds much complexity, associated with phase changes, its effect on atmospheric stability and the release of latent heat during condensation. Here, we take an important step towards incorporating moisture into our understanding of mid-latitude dynamics by reconciling two diverging lines of literature, which suggest that atmospheric moisture can either increase or decrease mid-latitude eddy kinetic energy. We explain this divergence by showing that moisture makes individual eddies more energetic, but also makes the environment in which eddies form less favorable for eddy growth. In Earth-like climates, the latter effect wins out such that moisture decreases atmospheric eddy kinetic energy. We demonstrate this point using several different idealized atmospheric models, which allow us to gradually add complexity and also to smoothly vary between moist and dry climates. These results add fundamental understanding to how moisture affects mid-latitude climates, including how its effects change in warmer and moisture climates, while also highlighting some drawbacks of the idealized atmospheric models.

1. Introduction

Much of our understanding of mid-latitude dynamics comes from dry models of the atmosphere. Both individual weather systems and the mean state of the mid-latitude atmosphere can be usefully studied while neglecting atmospheric water vapor, which eliminates the complications of phase changes and associated latent heat release. But despite the advantages of this simplification, it is clear that moisture does affect mid-latitude eddy activity. Idealized calculations show that latent heat release increases the linear growth rate and kinetic energy of moist baroclinic eddies (Bannon 1986; Emanuel et al. 1987; Gutowski et al. 1992; Zurita-Gotor 2005; Kohl and O'Gorman 2022; Brown et al. 2023), while simulations of individual events have demonstrated the crucial role of latent heating in storm intensification (Reed et al. 1988; Wernli et al. 2002; Joos and Wernli 2012). Ignoring the reduced static stability in the presence of moisture causes models to underestimate the eddy kinetic energy (EKE) of the storm tracks (Chang 2006; O'Gorman 2011), and Chang et al. (2002) further showed that moisture contributes positively to the budget of eddy available potential energy (EAPE) in reanalysis data. Long before these results, Lorenz (1979) found that the mean available potential energy (MAPE) of the atmosphere is always greater when the potential release of latent heat due to condensation of water vapor is taken into account, though the precise relationship between moist MAPE and EKE is still unclear.

On the other hand, studies of both idealized atmospheric general circulation models (GCMs, see O'Gorman and Schneider 2008; Schneider et al. 2010b) and comprehensive climate models and reanalysis data (O'Gorman 2010; Gertler and O'Gorman 2019) have found that mid-latitude EKE scales linearly with the dry MAPE, which maximizes in climates similar to that of Earth's present day and decreases in warmer – and moister – climates. In more direct tests, simulations with idealized GCMs have found that increasing atmospheric moisture while keeping temperature fixed decreases mid-latitude EKE (Frierson et al. 2006; Bembenek et al. 2020; Lutsko and Hell 2021). Bembenek et al. (2020) analyzed the energy budget of their two-layer moist shallow water simulations and found that precipitation acts as an energy sink, leaving less energy that can be converted from MAPE into EAPE, and in turn from EAPE into EKE.

So there is compelling evidence that moisture may either increase or decrease mid-latitude EKE. In this study, we reconcile these opposing results by drawing a distinction between moisture's effects on individual eddies – which it makes more energetic – and its effects on the large-scale conditions in which eddies form – which it makes less favorable for eddy growth. In all of the situations we consider, the latter effect wins out, such that including moisture increases the EKE for a given environment or a given storm, but weakens EKE when environmental conditions are allowed to vary.

We demonstrate how moisture's impact on EKE depends on the large-scale environment using simulations with a hierarchy of idealized atmospheric models in which atmospheric moisture is systematically varied between the moist and dry limits. We begin with a moist, two-layer quasi-geostrophic (QG) model. Two-layer QG models have played a fundamental role in our understanding of mid-latitude dynamics, and are commonly run in either homogeneous set-ups with fixed, uniform baroclinicity (e.g., Haidvogel and Held 1980; Panetta 1993; Pavan and Held 1996; Held and Larichev 1996), or in channel configurations, in which the mean flow is relaxed to an equilibrium profile but is otherwise free to evolve (e.g., Lee and Held 1993; Zurita-Gotor et al. 2014; Zurita-Gotor 2014; Lutsko et al. 2015, 2017). Most previous work on 2-layer QG models has focused on dry models, but Lapeyre and Held (2004) introduced a moist homogeneous version of the model, which Lutsko and Hell (2021) extended to a channel geometry (see also Bouchet et al. 2009; Laîné et al. 2011; Lambaerts et al. 2011a,b, 2012, for studies of moist 2-layer shallow water models). By running simulations in both set-ups we show that in the same dynamical system, moisture can either increase EKE (in the homogeneous case with fixed baroclinicity) or decrease EKE (in the channel case when the baroclinicity can adjust).

The suitability of 2-layer QG models for studying moist processes is still an open question, so we have also studied a moist, gray radiation GCM, which has been widely used by the atmospheric dynamics community (e.g., Frierson et al. 2006, 2007; O'Gorman and Schneider 2008a,b; Schneider et al. 2010a; Levine and Schneider 2015; Bischoff and Schneider 2016; Lutsko and Popp 2018; Wills and Schneider 2018; Lutsko et al. 2019). The stratification has more freedom to respond to changing thermodynamic conditions in the gray radiation GCM than in the QG model, and the GCM includes other dynamically relevant factors, such as the tropopause height, which are not represented in the two-layer QG model. Since the GCM uses a fixed profile of longwave optical depths, it can be smoothly varied between the moist and dry limits; in a model with an active water vapor feedback the effects of atmospheric moisture would have to be separated from large global-mean warming and cooling of the model.

Mid-latitude EKE decreases as moisture is added to the GCM, which we investigate by examining changes in MAPE and by considering the GCM's energy budget (also known as the Lorenz Energy Cycle). As mentioned above, previous studies have found a linear relationship between MAPE and mid-latitude EKE in simulations mimicking changes in atmospheric CO_2 concentrations, so we begin by analyzing how MAPE changes when moving between dry and moist climates. Next, we calculate the terms in the energy budgets of the simulations, which highlights the importance of latent heat release in driving eddy activity at mid-latitudes, especially the location where latent heat release occurs. Comparing the moist GCM to the QG model also reveals key drawbacks of the latter for studying moist dynamics. Most strikingly, the energy cycles of the moist GCM simulations resemble the "strong moisture" regime of the QG model, in which the flow is characterized by strong low-level cyclones and weak upper-level anticyclones. Although the flow in the strong moisture regime is qualitatively different from what is observed in Earth's mid-latitudes (it is more reminiscent of the "TC-Worlds" seen in simulations of rotating radiative-convective equilibrium; e.g., Held and Zhao (2008); Zhou et al. (2017)), from an energetic perspective, at least, this regime seems to be a closer analogue to Earth's atmosphere than QG simulations with weak latent heating.

Finally, an alternative way of constraining mid-latitude EKE is by using the atmosphere's entropy budget, and the related concept of atmospheric work (defined more fully in section 5). While these concepts can only be used to constrain the total kinetic energy of the atmosphere, rather than the EKE, they have been used by Laliberté et al. (2015) to explain the slow-down of the large-scale circulation under warming. There is ambiguity concerning how to calculate some of the terms in the moist GCM's entropy budget, so we have not attempted to close this budget. Instead, we place our results in the context of previous work on atmospheric entropy budgets, and speculate on how moisture likely affects the terms in the GCM's entropy budget.

The rest of the paper is structured as follows. In sections 2 and 3 we describe and analyze the homogeneous and channel configurations of the moist QG model, respectively. The moist GCM simulations are presented and analyzed in section 4, then in section 5 we discuss the relationships between EKE, work and the entropy budget of the moist GCM. We end with conclusions in section 6.

2. Homogeneous Quasi-Geostrophic Model

a. Model description

The homogeneous moist QG model numerically solves the system first proposed by Lapeyre and Held (2004), which consists of two constant density layers on a β-plane in a doubly-periodic domain, with moisture added as an active tracer in the lower layer. The zonal-mean winds vary linearly in the y-direction, such that the zonal-mean potential vorticity (PV) gradient in each layer is $Q_k = \beta + (-1)^{k+1}U$, where $U_1 = -U_2 = U/2$ and $k = 1$ in the upper layer and $k = 2$ in the lower layer. Ekman friction is added to the lower layer.

The (non-dimensionalized) dynamical equations in this system follow PV anomalies:

$$\begin{aligned}\frac{\partial}{\partial t}q_k(x,y,t) + J(\psi_k(x,y,t), q_k(x,y,t)) =& (-1)^k \frac{\partial}{\partial x}q_k(x,y,t) - (\beta - (-1)^k)\frac{\partial}{\partial x}\psi_k(x,y,t) \\ &- \frac{1}{\tau_f}\delta_{k2}\nabla^2\psi_k(x,y,t) + (-1)^k LP(x,y,t) - \nu\nabla^4 q_k(x,y,t),\end{aligned} \tag{1}$$

where $q_k = \nabla^2\psi_k + (-1)^k(\psi_1 - \psi_2)$ is the spatially-varying PV anomaly in each layer; the ψ_ks are the streamfunctions; J is the Jacobian operator; τ_f is a frictional time-scale acting only in the lower layer; and ν is a hyper-diffusion coefficient. L is the non-dimensionalized latent heat of vaporization and P is the anomalous precipitation (see below). The reader is referred to Lapeyre and Held (2004) for a full derivation.

Moisture is represented as a non-dimensionalized mixing ratio, and is decomposed into a domain-mean mixing ratio M and an anomalous mixing ratio m. M evolves as

$$\frac{\partial M(t)}{\partial t} = E - \Pi(t), \tag{2}$$

where E is a specified, constant domain-mean evaporation rate and Π is the domain-mean precipitation. The anomalous moisture evolves as

$$\begin{aligned}\frac{\partial}{\partial t}m(x,y,t) + J(\psi_2(x,y,t), m(x,y,t)) = \frac{1}{2}\frac{\partial}{\partial x}m(x,y,t) + C\frac{\partial}{\partial x}\psi_2(x,y,t) - P(x,y,t) \\ - \nabla\cdot\mathbf{u_2}(x,y,t),\end{aligned} \tag{3}$$

where C is a constant that relates the saturation mixing ratio (m_s) and the temperature ($\psi_1 - \psi_2$) in a linearization of the Clausius-Clapeyron relation: $m_s \equiv C(\psi_1 - \psi_2)$. The last term on the right hand side of equation 3 is a linearization of ageostrophic advection in the lower layer.

The total precipitation at a grid-point is equal to $\Pi + P$, and instantaneously resets $(1+CL)M + m$ to the saturation mixing ratio whenever it rises above this value. The addition of moisture and precipitation complicates the numerics of the model, and we follow the approach described in the appendix of Lapeyre and Held (2004) to calculate the precipitation and $\nabla\cdot\mathbf{u_2}$ (see also Lutsko and Hell 2021).

We have run linear and nonlinear experiments with this model on a grid of size $10\pi\times 10\pi$, with 256 gridpoints in each direction. The linear experiments allow us to estimate eddy growth rates, which can be compared to previously derived scalings, while the nonlinear experiments show how EKE depends on moisture in this system. In the linear experiments, nonlinear eddy interactions are turned off and small scale noise is added to the streamfunction and moisture fields to initiate instability. These experiments are run for 100 model time-units, with averages taken over the last 50 model time-units (1 time-unit ≈0.2 Earth days). The nonlinear experiments are run for 2000 model time-units, with the first 1000 time-units discarded as spin-up.

Our default parameters are $\beta = 0.78$, $L = 0.2$, $C = 2$ and $E = 1.39$, again following Lapeyre and Held (2004). We have run linear and nonlinear experiments with L varied from 0 to 0.99, holding $C = 2$, and with C ranging from 0 to 4, holding $L = 0.2$. These can be thought of, roughly, as varying the strength of latent heating and varying the rate at which atmospheric water vapor increases with warming, respectively, though the non-dimensional L and C both depend on the dimensional latent heat of vaporization. We have also varied the evaporation rate, E, but for ease of presentation focus here on the experiments with varying L and C. For our control value of $E = 1.39$ the model is close to saturation throughout most of the domain, with a domain-averaged relative humidity of about 0.8.

b. Linear and nonlinear simulations

In the linear simulations the eddy growth rate (σ) increases monotonically with L, from roughly 0.12 for $L = 0$ to roughly 0.36 for $L = 0.99$ (Figure 1a[1]), consistent with past work suggesting that latent heat release increases eddy growth rates. Zurita-Gotor (2005) derived a scaling for eddy growth rates in moist QG systems which predicts that σ decreases with the effective stability, r:

$$\sigma = \frac{-(r+1)+\sqrt{(r+1)^2+4r}}{2r}. \tag{4}$$

An effective stability can be defined for our system as $r = \frac{1-L}{1+CL}$ (Lapeyre and Held 2004), and the red curve in Figure 1b shows that equation 4 produces an excellent match to the simulated growth rates, as the growth rate increases rapidly as the effective stability decreases. Equation 4 works well despite being derived on an f-plane, rather than a β-plane (as used here). We note that Emanuel et al. (1987) derived a different scaling for moist growth rates in a semigeostrophic system, but their scaling does not match the results here well (Figure 1a of Zurita-Gotor (2005) provides a comparison of the two scalings). Qualitatively, the Emanuel et al. (1987) prediction is similar: eddy growth rates increase as the effective stability decreases.

The non-linear simulations show that EKE also increases with L in this system (Figure 1c), and similar results are seen in the experiments in which C is varied (triangles in Figure 1d). If eddy length-scales are assumed to be constant, then the EKE should scale as σ^2, and we confirm in Figure 1d that equation 4 provides a good fit to the simulated EKE in both the simulations with

[1]Growth rates are calculated as $\sigma = \log(|\psi_1^t|_1/|\psi_1^{t-1}|_1)/\Delta t$.

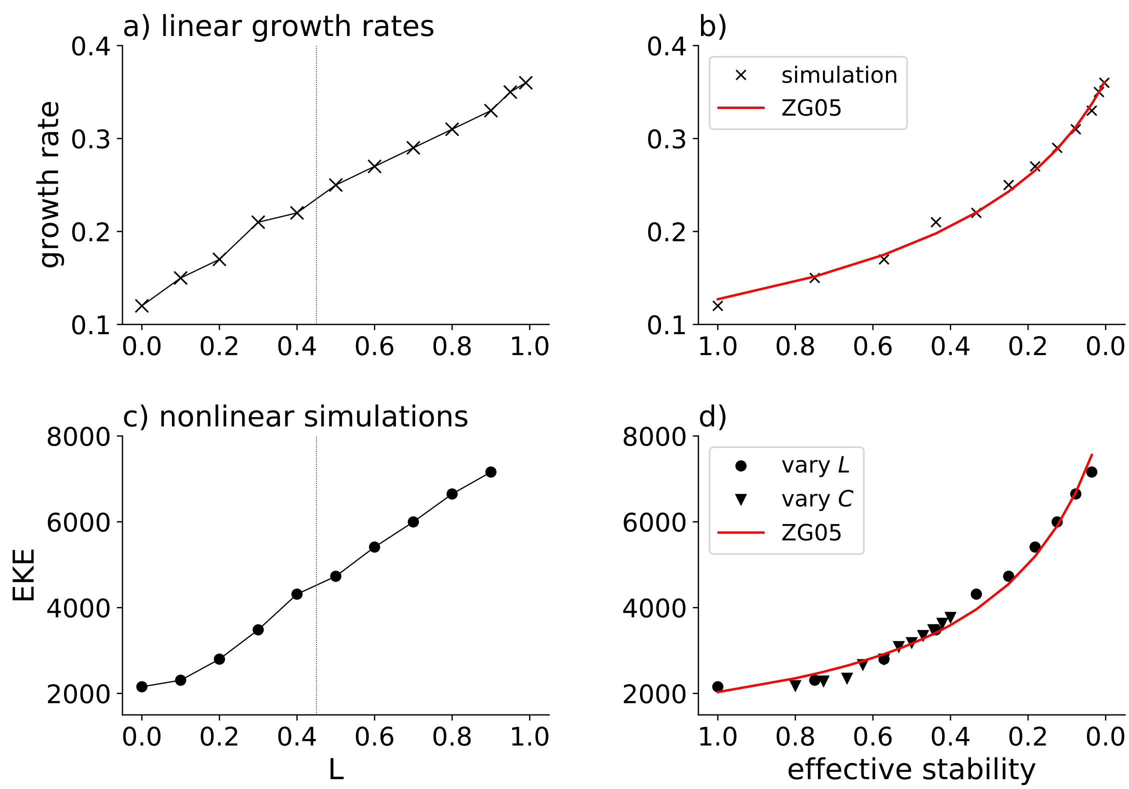

FIG. 1. Results of the homogeneous QG calculations. Top row: Eddy linear growth rate as a function of L (a) and as a function of the effective stability r (b). The red curve shows the growth rates predicted by equation 4. Bottom row: domain-averaged EKE in the nonlinear simulations as a function of L (c) and as a function of effective stability (d). In panel d) the red curve shows the EKE predicted by equation 4, assuming eddy length-scales stay fixed and with the y offset fit to minimize the RMSE. The triangles show the results of simulations in which C is varied and L is kept fixed at 0.2. The dotted lines in the left panels mark the transition from the “weak" to the “strong" moisture regime.

varying L and with varying C (we experimented with other integer powers of σ and confirmed that the square does give the best fit). As L is increased the model transitions to the “strong moisture" regime described in the introduction, which is a qualitatively different climate state to the dry and “weak moisture" climates, but the σ^2 scaling appears to hold robustly across the transition.

These simulations demonstrate that when baroclinicity is fixed, linear growth rates and EKE increase when moisture is added to the moist QG model, closely following the scaling derived by Zurita-Gotor (2005). Hence for fixed environmental conditions, moisture increases the EKE of QG systems.

3. Channel Quasi-Geostrophic Model

a. Model description

The channel QG model was described in Lutsko and Hell (2021). It also consists of two constant density layers on a β-plane, but the interface between the layers is relaxed to a baroclinically-unstable radiative-equilibrium slope, producing a strong zonal jet in the center of the domain. Sponges at the meridional boundaries damp eddy activity, creating a channel geometry.

The non-dimensionalized equations of motion are now written in terms of the total potential vorticity

$$\begin{aligned}\frac{\partial}{\partial t}Q_k(x,y,t)+J(\Psi_k(x,y,t),Q_k(x,y,t)) = &-\frac{1}{\tau_d}(-1)^k(\Psi_1(x,y,t)-\Psi_2(x,y,t)-\Psi_R(y)) \\ &-\frac{1}{\tau_f}\delta_{k2}\nabla^2\Psi_k(x,y,t)+(-1)^k L\mathcal{P}(x,y,t)-\nu\nabla^4 Q_k(x,y,t),\end{aligned} \tag{5}$$

where $Q_k = \nabla^2\Psi_k + (-1)^k(\Psi_1 - \Psi_2) + \beta y$, τ_d is a Newtonian relaxation time scale and Ψ_R is the radiative-equilibrium interface slope, described in Lutsko et al. (2015). The channel model tracks a single moisture variable, $\mathcal{M}$:

$$\frac{\partial}{\partial t}\mathcal{M}(x,y,t)+J(\Psi_2(x,y,t),\mathcal{M}(x,y,t)) = \mathcal{E}(x,y,t)-\mathcal{P}(x,y,t)-\nabla\cdot\mathbf{u_2}(x,y,t), \tag{6}$$

where $\mathcal{E}$ and $\mathcal{P}$ represent the total evaporation and precipitation, rather than anomalies. Precipitation instantaneously resets $\mathcal{M}$ to the saturation mixing ratio $\mathcal{M}_s \equiv C(\Psi_1 - \Psi_2)$ wherever $\mathcal{M} > \mathcal{M}_s$:

$$\mathcal{P} = \begin{cases}(\mathcal{M}-\mathcal{M}_s)/\tau_p, & \text{if } \mathcal{M} > \mathcal{M}_s, \\ 0 & \text{if } \mathcal{M} \leq \mathcal{M}_s,\end{cases} \tag{7}$$

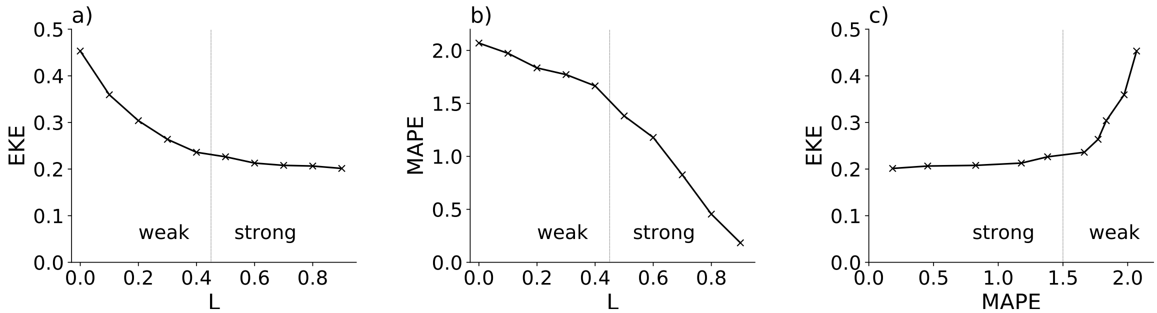

Fig. 2. a) EKE as a function of L in the moist QG channel simulations. b) MAPE as a function of L in the same simulations. c) EKE as a function of domain-averaged MAPE in the same simulations. Both the EKE and the MAPE are calculated by averaging over the baroclinic regions (see text for more details). The dotted lines mark the transition from the “weak" to the “strong" moisture regime, as indicated by the text on each panel.

with τ_p set to 1, and evaporation is calculated using a “bulk formula" wherever the moisture is subsaturated:

$$\mathcal{E} = \begin{cases} \hat{\mathcal{E}}|\mathbf{U_2}|(\mathcal{M}_s - \mathcal{M}), & \text{if } \mathcal{M} < \mathcal{M}_s, \\ 0 & \text{if } \mathcal{M} \geq \mathcal{M}_s, \end{cases} \tag{8}$$

with $|\mathbf{U}_2|$ the absolute wind speed in the lower layer and $\hat{\mathcal{E}}$ a constant of proportionality.

We use the same model parameters and domain size as Lutsko and Hell (2021): the zonal width is 72 units and the meridional length is 96 units, with 128 wavenumbers retained in both dimensions. For the parameters not related to moisture we set $\beta = 0.2$, $\tau_f = 15$, $\tau_d = 100$ and $\nu = 10^{-6}$. For the moist parameters, we set $C = 2$ and $\hat{\mathcal{E}} = 0.1$, then vary L from 0 to 0.9.

b. Simulation results

The channel model exhibits the opposite behavior to the homogeneous model, as the EKE decreases monotonically with L, from 0.46 in the dry case, to just over 0.2 in the L = 0.9 case (Figure 2a). The largest decreases occur for $L < 0.4$, and the EKE only decreases slightly between $L = 0.5$ and $L = 0.9$. To understand the relationship between L and EKE in these simulations, we examine the terms in the Lorenz Energy Cycle (Lorenz 1955, Appendix A), especially the Mean Available Potential Energy (MAPE). If the supercriticality of the channel model is assumed fixed, then the MAPE should be linearly related to the EKE (Schneider and Walker 2006). The MAPE

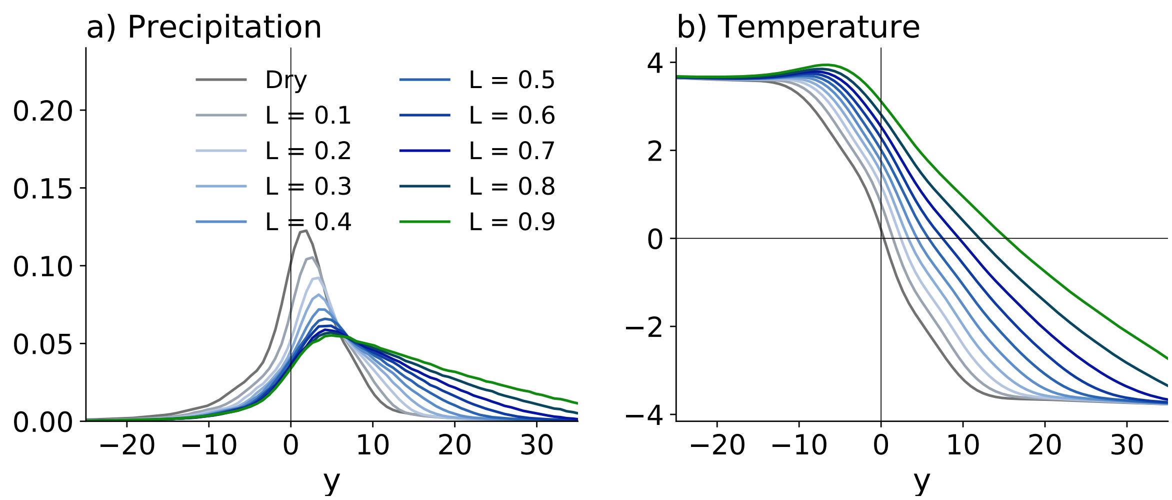

FIG. 3. a) Climatological, zonal-mean precipitation in the moist channel simulations. b) Climatological, zonal-mean temperature ($\Psi_1 - \Psi_2$) in the moist channel simulations.

also decreases monotonically with L (Figure 2b), but whereas the EKE is roughly constant at large L, the MAPE decreases more rapidly in the strong moisture regime ($L > 0.4$). Figure 2c shows that EKE is essentially independent of the MAPE in the strong moisture regime (the transition between the weak and strong moisture regimes can be diagnosed by examining power spectra of EKE, which exhibit maxima at the typical scale of the lower-layer cyclones for large L, not shown). Transitioning to the strong moisture regime appears to cause a qualitative change in the relationship between EKE and MAPE, so we will examine the weak and strong moisture simulations separately.

In the weak moisture regime, the MAPE decreases with increasing L because precipitation tends to form on the poleward side of the jet (Figure 3a, see also Figure 1 of Lutsko and Hell (2021)). Latent heat is released where the model is relatively cool, weakening the meridional temperature gradient (Figure 3b) and lowering the MAPE. This is the primary reason for the reduction in EKE with L, but there is also a notable decrease in EKE between the dry and $L = 0.1$ cases – more than would be expected from a linear regression of MAPE onto EKE in this regime (not shown). We have traced the additional decrease to precipitation's role as a sink of MAPE when latent heating is weak (crosses in Figure 4b), reducing the conversion to EAPE compared to the dry case. Precipitation was also a sink of MAPE in the comparison of dry and moist shallow water simulations in Bembenek et al. (2020). It contributes weakly to the EAPE budget for small L, which Bembenek et al. (2020) showed is due to precipitation being out of phase with temperature in

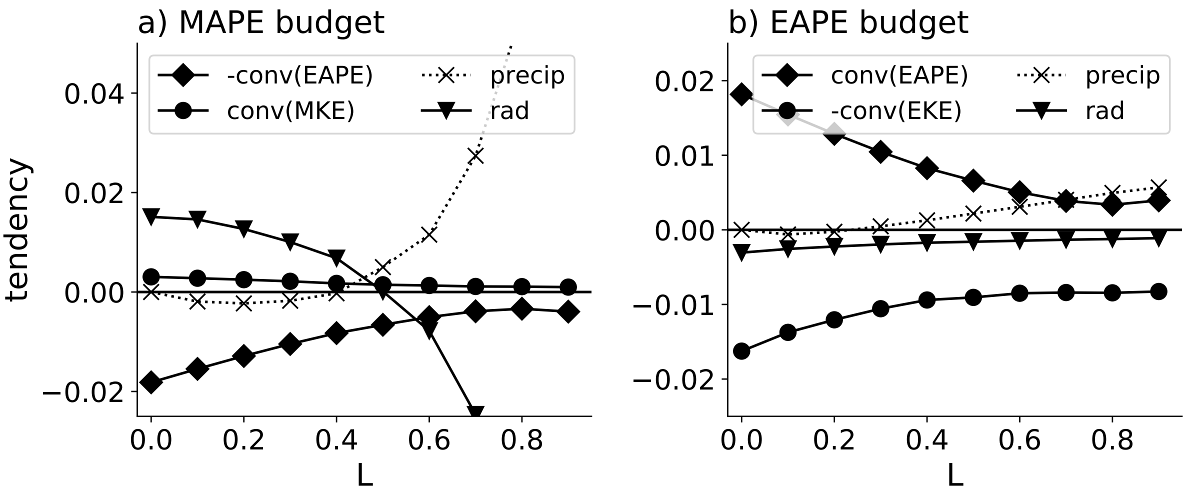

FIG. 4. a) Terms in the MAPE budget of the moist QG channel simulations. b) Terms in the EAPE budget of the moist QG channel simulations. Note the different y-axes scales.

this regime. Note that we have calculated all energy budget terms by averaging over the "baroclinic zone", which we define as where the lower layer mean PV gradient is negative. We obtain similar results when averaging over the whole domain, but prefer to restrict our focus to the baroclinic zone to avoid the sponge regions at the edges of the domain. Bembenek et al. (2020) calculated their energy budgets using global integrals.

In the strong moisture regime both precipitation terms are sources of potential energy (crosses in Figure 4), and the leading balance in the MAPE budget is between precipitation and radiation. In this regime, the combination of latent heating and eddy heat fluxes cause the model to be anomalously warm up to $y = +20$ (Figure 3b), but the largest temperature gradients are still at relatively low latitudes (e.g., the jet is centered near $y = +5$, not shown), such that the majority of eddy activity is in the relatively warm region between $y = 0$ and $+20$. Most of the precipitation also occurs in these latitudes, such that the associated latent heat release now heats a relatively warm region.

These simulations resemble a climate in which the strongest temperature gradients are located in the warm subtropics, as are the eddy-driven jet and the majority of the eddy activity. Higher latitudes have relatively weak temperature gradients and are quiescent compared to the subtropics, though passing storms occasionally bring precipitation. The MAPE budget is a balance between latent heat release, which warms the subtropics and increases the MAPE, and radiation, which cools the subtropics and becomes a sink of MAPE. A small residual is left over to be converted into EAPE. In our simulations, the residual saturates for strong latent heating, such that the energy available to be converted into EKE is roughly constant for $L \geq 0.5$.

Precipitation becomes a source of EAPE in the strong moisture regime (Figure 4b), as latent heat is released in the cores of the warm cyclones which dominate these climates, but this term is small compared to precipitation's zonal-mean contribution. We have not investigated the cyclones in further detail, but note that they resemble the diabatic Rossby vortices analyzed by Kohl and O'Gorman (2022).

4. Moist Gray Radiation Model

a. Model description

The moist, gray radiation GCM was first described by Frierson et al. (2006). It solves the primitive equations on the sphere and is forced by a gray radiation scheme. The GCM is coupled to a slab ocean of depth 1m, with no representation of ocean dynamics or sea ice, and the model includes the simplified Betts-Miller (SBM) convection scheme of Frierson (2007). A mixed-layer depth of 1m was used so that the model would spin up quickly, while leaving the resulting mean climate the same as for larger mixed layer depths. We show results using a convective relaxation time-scale τ_{SBM} of 2 hours and a reference relative humidity $RH_{\mathrm{SBM}} = 0.7$. The boundary layer scheme is the one used by O'Gorman and Schneider (2008a). In every experiment the GCM was integrated at T85 truncation (corresponding to a resolution of roughly 1.4° by 1.4° on a Gaussian grid) with 30 vertical levels extending up to 16hPa, starting from a state with uniform SSTs.

To vary the moisture in the model, we follow Frierson et al. (2006) and multiply the saturation vapor pressure by a constant factor γ:

$$e_s^*(T,\gamma) = \gamma e_{s0}^*(T), \tag{9}$$

where e_{s0}^* is the model's default saturation pressure. We ran an initial set of simulations in which γ was varied from 0 (i.e., the model is dry) to 1 in increments of 0.2 then, motivated by a desire to further probe the dry-moist transition, we ran an additional set of simulations with γ set to 10^{-3}, 10^{-2} and 10^{-1}. All simulations were run for 2000 days, with averages taken over the final 1500 days, and we will present simulations with equinoctial solar forcing, so all data are symmetrized about the equator.

b. Eddy kinetic energy across climates

As in the channel QG model simulations, the EKE decreases as the GCM transitions from dry to moist, from almost 1MJm^{-2} in the dry case to ~0.8 MJm^{-2} for $\gamma = 1$ (Figure 5a). The decrease is roughly exponential in γ, and the EKE appears to saturate for large γ. We investigate these changes first by comparing with changes in MAPE and then by examining the terms in the Lorenz Energy Cycle in the simulations.

1) EKE and MAPE

Previous work has suggested that mid-latitude EKE follows the MAPE, such that whatever drives changes in MAPE explains EKE changes. In the GCM simulations, the MAPE also decreases exponentially with γ, from over 10MJm^{-2} in the dry simulation to just over 2.5MJm^{-2} for $\gamma = 1$ (Figure 5b), and plotting the EKE against the MAPE reveals the existence of two regimes: a "dry" and a "moist" regime, with the transition near $\gamma = 0.2$. In each regime the EKE is roughly linear in MAPE, but the slope is substantially smaller in the dry regime (i.e., the EKE increases more slowly for a given change in MAPE). This suggests that MAPE is converted into EKE less efficiently in the dry regime.

We return to the transition between the dry and moist regimes below, and focus first on understanding the changes in MAPE. The MAPE values indicated by the black crosses in Figure 5 were calculated following the original formulation in Lorenz (1955), which is difficult to interpret. An approximate form of Lorenz's dry MAPE was derived by Schneider and Walker (2008), which allows the drivers of changes in MAPE to be diagnosed:

$$\mathrm{MAPE} \approx \frac{c_p}{24g} < \bar{p}_s - \bar{p}_t > \Gamma < \partial_y \bar{\theta} >^2 L_z^2, \tag{10}$$

where c_p is the heat capacity of dry air, g is the gravitational acceleration, p_s is surface pressure, p_t is the pressure of the tropopause, θ is potential temperature and L_z is the width (in meters) of

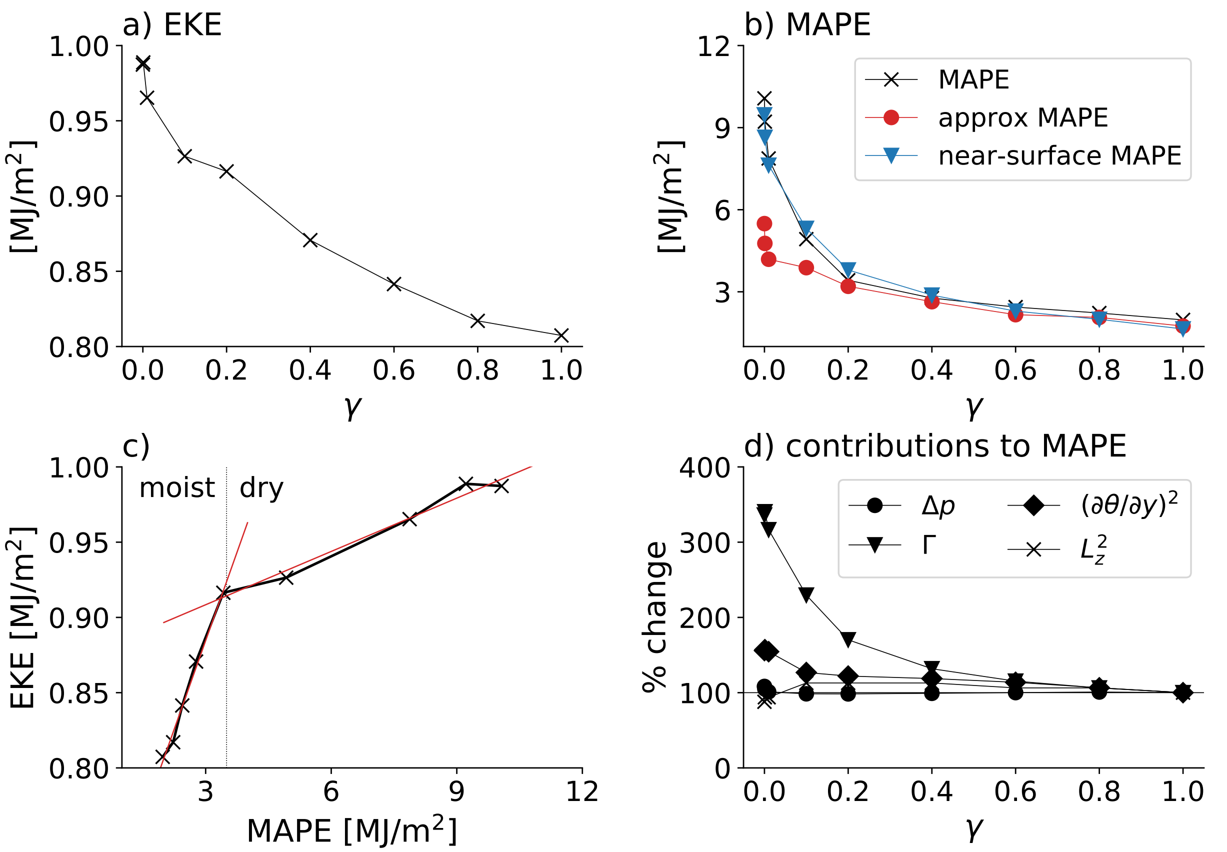

FIG. 5. a) EKE as a function of γ in the moist GCM simulations. b) MAPE as a function of γ in the moist GCM simulations. The black crosses show the true MAPE, the red circles the approximate MAPE (equation 10) with terms calculated by integrating over the depth of the troposphere, and the blue triangles show the approximate MAPE with terms calculated using near-surface quantities. c) EKE versus MAPE in the same simulations. The vertical black dashed line approximately separates the "moist" and "dry" regimes, based on MAPE and EKE, and the solid red lines show linear least-squares fits to the data in the two regimes. d) Contributions of different terms in equation 10 to the near-surface approximate MAPE in the same simulations (blue triangles in panel b), with each term normalized by its value for $\gamma = 1$.

the baroclinic zone. Γ represents an inverse stability:

$$\Gamma = -\frac{\kappa}{p_0} < \overline{\partial_p \theta} >^{-1}, \tag{11}$$

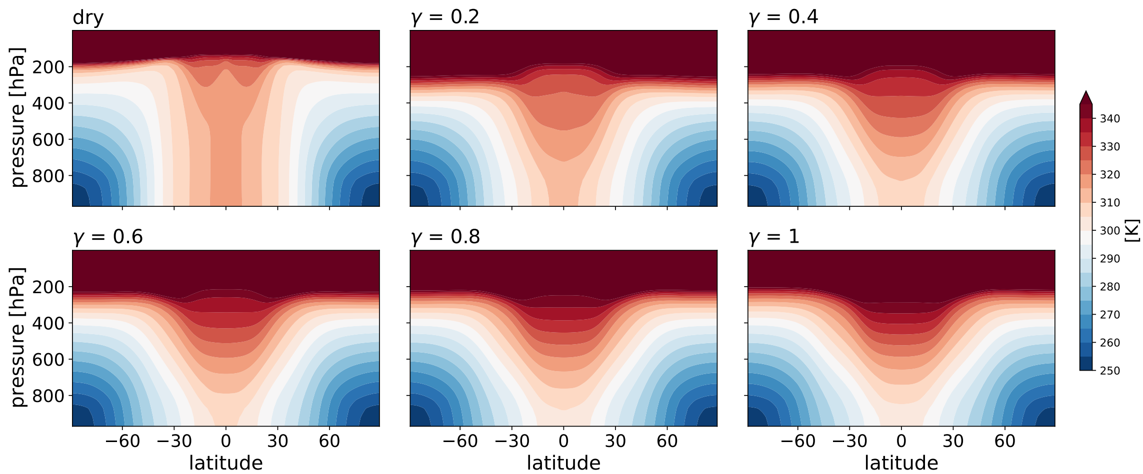

Fig. 6. Climatological zonal-mean potential temperatures as a function of latitude and pressure in the six moist GCM simulations with γ varied in increments of 0.2.

where $\kappa = R_d/c_p$, with R_d the dry gas constant and p_0 a reference pressure. Overbars denote time averages and angle brackets denote averages over the baroclinic zone. We set c_p = 1005Jkg^{-1}K^{-1}, g =9.8ms^{-2}, κ = 2/7 and p_0 = 1000hPa in all calculations[2].

The approximate MAPE allows us to identify what causes the MAPE to decrease as moisture is added to the model. Comparing the terms in equation 10 shows that the most important factor is the inverse stability Γ, with the meridional surface temperature gradient also contributing to increases in MAPE (Figure 5d). Examining the climatological potential temperature in the initial six simulations confirms the stability increases as moisture is added to the model (Figure 6): in the dry case the isentropes are vertical in most of the mid-latitude troposphere, and they become more sloped as moisture is added. We also note that the meridional temperature gradients go to zero in the upper troposphere of the driest simulations (see e..g, near 400hPa in the top left of Figure 6), which may explain why the lower tropospheric MAPE is a better approximation to the true MAPE.

[2]There is ambiguity over whether the terms involving potential temperature should be evaluated in the lower troposphere only or over the depth of the entire troposphere. Schneider and Walker (2008) originally suggested taking lower tropospheric values (e.g., averages over 800-700hPa), but O'Gorman and Schneider (2008) later proposed averaging over the depth of the troposphere to account for latent heat release aloft. The red and blue lines in Figure 5b show that using the lower troposphere MAPE produces a closer match to the true MAPE, and we have used the lower tropospheric form in our interpretation. We caution, however, that the vertically-averaged form of MAPE was designed for moist climates, and for the larger values of γ shown here the two approximations are in close agreement. For other simulations, designed to investigate global warming for example, taking a vertical integral may be more appropriate.

There is also ambiguity as to how to define the baroclinic zone. In the original formulation it was defined as the region where the eddy potential temperature flux at 840hPa was within 30% of its maximum (Schneider and Walker 2006), whereas O'Gorman and Schneider (2008) suggested defining it as the latitudes within 15° of the maximum vertically-integrated eddy potential temperature flux. We have calculated the approximate MAPE using both definitions, and find that our results are qualitatively insensitive to this choice (not shown), and the results presented here use the Schneider and Walker (2006) definition, but with the threshold set to 50% which we find gives more robust estimates.

The vertical isentropes in the dry simulation suggest that the stability in this model is largely set by convection, as was noted by Frierson et al. (2006). We have experimented with strengthening the midlatitude baroclinicity by increasing the parameter controlling the equator-to-pole insolation gradient (Δ_s in Frierson et al. (2006)) from 1.4 to 1.8, but even in this set-up the isentropes are essentially vertical in the midlatitudes of a dry simulation (not shown). We are unsure how to avoid producing vertical isentropes in dry simulations, but note that Schneider and O'Gorman (2008) found that extratropical stratification scales with convective lapse-rate in a dry model, even when the stability is clearly set by eddy fluxes (see their Figure 4). The decrease in the meridional temperature gradient is also large enough that even without the stability changes, the EKE would decrease in moister climates (diamonds in Fgure 5d).

2) Lorenz Energy Cycle

The results of the previous section suggest that increases in stability are the primary cause of the reductions in EKE as moisture is added to the GCM, but also demonstrate the limitations of using MAPE to explain EKE variations. In both regimes the linear fit is approximate, while the very weak stabilities in the dry simulations may push beyond the bounds in which the concept of MAPE is appropriate. As an alternative approach to understanding the changes in EKE, we examine the terms in the Lorenz Energy Cycle, particularly the diabatic terms associated with latent heat release, radiative cooling and surface fluxes. While the Lorenz Energy Cycle has been well studied in idealized models and reanalysis data (e.g., Li et al. 2007; Kim and Kim 2013; Chai et al. 2016; Pan et al. 2017; Lembo et al. 2019), the diabatic terms have received relatively little attention (though see Romanski and Rossow 2013). These can be calculated as (Lorenz 1955):

$$G_Z = \frac{-1}{g}\int_0^{ps}\left(\frac{p_s}{p}\right)^{\kappa}\Gamma < T^* Q_L^* > dp, \tag{12a}$$

$$G_E = \frac{-1}{g}\int_0^{ps}\left(\frac{p_s}{p}\right)^{\kappa}\Gamma < T' Q_L' > dp, \tag{12b}$$

where Q denotes a diabatic heating, asterisks denote stationary anomalies from the time-and meridional averages, dashes denote transient anomalies and angle brackets again denote horizontal averages over the baroclinic zone. G_Z is the contribution to the MAPE budget and G_E is the contribution to the EAPE budget. We have calculated the contribution of latent heating ($G_{Z,P}$ and

$G_{E,P}$) explicitly and the contribution of diabatic terms not associated with latent heating ($G_{Z,NP}$ and $G_{E,NP}$) as residuals from the energy budgets.

The MAPE and EAPE budgets are plotted as functions of γ in Figure 7 (the conversion terms are calculated following Lorenz (1955) and all terms are calculated over the baroclinic zones described in the footnote above). For $\gamma \geq 0.1$, the MAPE budget is largely a balance between latent heating, which is a source of MAPE, and radiative cooling, which is a sink of MAPE. The conversions to EAPE and to Zonal Kinetic Energy (ZKE) balance the residual net diabatic heating, and are substantially smaller than either of the individual diabatic terms. These results are consistent with the observational analysis of Romanski and Rossow (2013), as well as the balance seen in the "strong moisture" QG simulations. From this perspective, a moist mid-latitude atmosphere can be interpreted as being in radiative-convective equilibrium when averaged over large enough scales. By contrast, in the dry regime the circulation is driven by strong surface sensible heat fluxes at low latitudes (included in $G_{Z,NP}$), which corresponds more closely to the conventional picture of the mid-latitude circulation as being driven by low latitude heating (see e.g., Chapter 10 of Holton and Hakim 2013). The transition from dry to moist occurs when latent heating replaces sensible heating as the leading driver of the MAPE budget, near $\gamma = 0.1$. We discuss the dry-to-moist transition further in the next section.

It is surprising that the latent heating contribution weakens as the atmosphere moistens. Examining the zonal-mean latent heating shows that this reflects the migration of the location of the maximum extratropical condensation to higher latitudes as γ is increased (Figure 8; we do not show it, but the maximum precipitation also moves to higher latitudes). For example, in the $\gamma = 0.2$ case, the maximum heating is found in the subtropics, where the atmosphere is already warm, and acts as a strong source of MAPE, whereas in the $\gamma = 1$ case the latent heating maximizes near 42°, where the atmosphere is relatively cooler (compare middle panel of top row and rightmost panel of bottom row in Figure 8). We are currently investigating the poleward shift of condensational heating, but note here that most of the evaporation still occurs in the subtropics, so the shift in the location of maximum latent heating reflects an increase in the distance water vapor is transported before it condenses out (or since its "time of last saturation"; c.f., Pierrehumbert et al. (2007); Sherwood et al. (2010)) as γ is increased. This could be related to changes in near-surface relative humidity or to the trajectories of individual air parcels. We have not investigated this in detail,

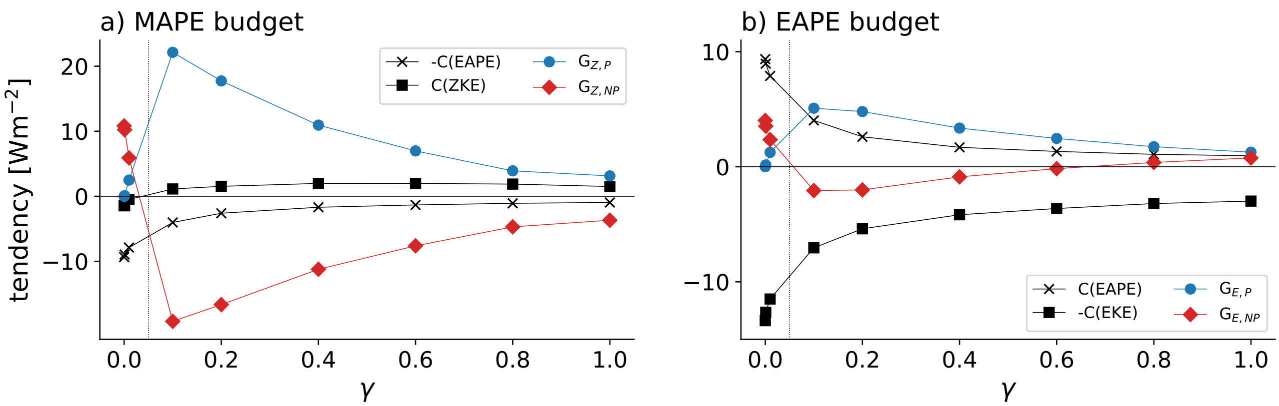

FIG. 7. a) Terms in the MAPE budget of the moist GCM simulations. b) Terms in the EAPE budget of the moist GCM simulations. $G_{Z,NP}$ and $G_{E,NP}$ denote contributions from diabatic heating not associated with latent heat release, which are calculated as residuals. Note the different y-axis scales. In both panels, the solid lines separate the moist and dry regimes, now defined in terms of whether latent heat fluxes or sensible heat fluxes drive the circulation.

though we have confirmed that the subtropical near-surface relative humidity is higher for small γ, so that parcels of water vapor carried on the same trajectory will condense out sooner than for large γ.

The MAPE budget thus provides a different perspective on the reduction in EKE with γ, and on the dynamics of the mid-latitudes more generally. The dry regime corresponds to the conventional picture of the atmosphere's circulation, in which low latitudes are warmed, mainly through surface sensible heat fluxes, and this generates kinetic energy. But when a small amount of moisture is added to the GCM (~10% of the moisture in the control climate) the sensible heat flux drops, and latent heat release becomes the leading term warming the atmosphere, balanced by radiative cooling. Thinking of the atmosphere as a heat engine driven by the temperature difference between where energy is input and where it is radiated away, adding moisture decreases the atmosphere's thermodynamic efficiency (it decreases this temperature difference) because the energy is input at the dewpoint temperature of the near-surface subtropical air, rather than the surface temperature (see also Romps 2008; Pauluis 2011; Bannon 2015). For $\gamma = 0.1$, moisture condenses close to where it is evaporated, and the climate is functionally similar to a dry atmosphere in which heat is input at the surface through sensible heat transfer (i.e., the subtropical dewpoint temperature is

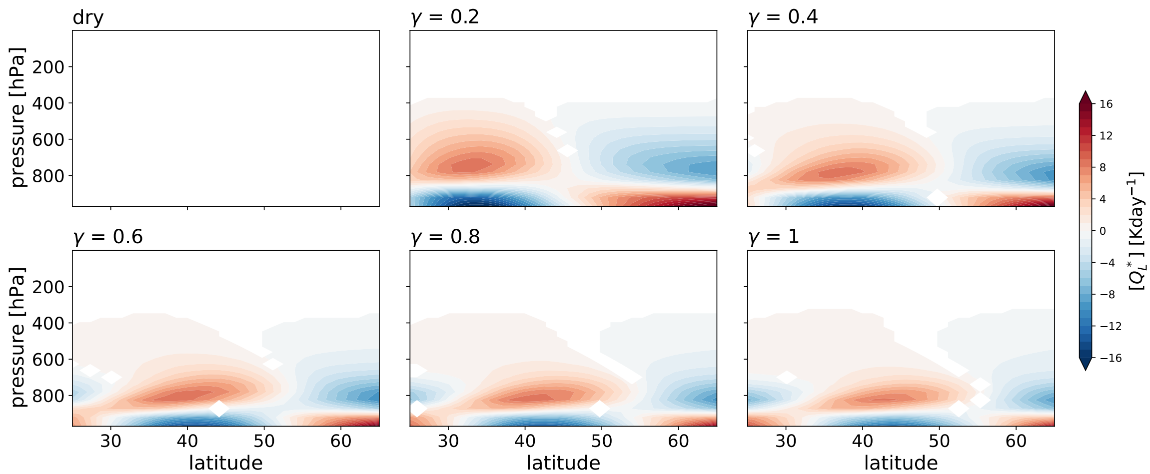

FIG. 8. Anomalous zonal-mean latent heating (Q_L^*) in the six moist GCM simulations with γ varied in increments of 0.2.

close to the near-surface temperature). For $\gamma = 1$ the moisture is transported a significant distance and the temperature difference is smaller. We return to the atmosphere's thermodynamic efficiency in section 5, below.

Finally, $G_{E,P}$ is a source of potential energy (Figure 7b), consistent with Chang et al. (2002), but it plays a much less important role than the zonal-mean latent heating. In the moist regime the conversion from MAPE to EAPE is roughly the same magnitude as $G_{E,P}$, and these together are balanced by the conversion to EKE. Interestingly, $G_{E,NP}$ switches from being a sink of EAPE for small γ to a source for $\gamma > 0.6$. As with the the $G_{Z,NP}$ term in the MAPE budget, this likely reflects an increased importance of the surface sensible heat flux.

c. The transition to the dry limit

The previous two sections suggest different definitions of the dry-to-moist transition. The relationship between EKE and MAPE exhibits a break between $\gamma = 0.1$ and $\gamma = 0.2$ (where the slope changes), while the MAPE budget indicates the transition occurs for $\gamma = 0.1$ (when latent heating takes over as the leading driver of the circulation). The former emphasizes differences in the efficiency with which the atmosphere converts MAPE into EKE, while the latter focuses on the driver of the flow, even if the impact on EKE is similar. The latter can also be stated in terms of

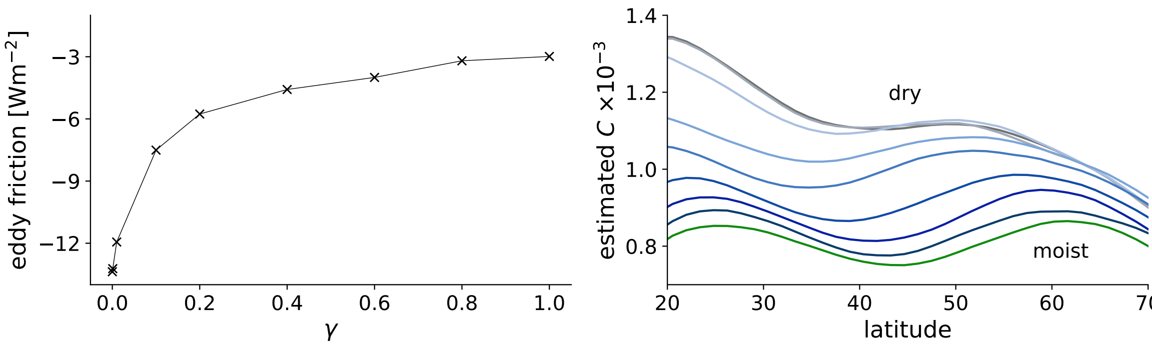

FIG. 9. a) Sink of EKE due to eddy friction in the moist GCM simulations. b) Effective drag co-efficients C in the moist GCM simulations, diagnosed from the time- and zonal-mean surface fluxes. γ increases going from the dark gray curve (labelled “dry") to the green curve (labelled “moist").

the Bowen Ratio:

$$\mathrm{Bo} \equiv \frac{\text{Sensible Heat Flux}}{\text{Latent Heat Flux}}, \tag{13}$$

where the MAPE budget says the transition occurs when the Bowen Ratio crosses 1.

To estimate the value of γ for which Bo = 1, we substitute bulk formulae for the fluxes and rearrange to give:

$$\mathrm{Bo} = \frac{c_p}{\gamma L_v}\left(\frac{\Delta q^*}{\Delta T} + \frac{q^*(T_a)(1-RH)}{\Delta T}\right)^{-1}, \tag{14}$$

where $\Delta T = T_s - T_a$ is the temperature difference between the surface and near-surface air, Δq^* is the difference in saturation mixing ratios associated with these temperatures and RH is the relative humidity of the near-surface air. The maximum Bowen ratio occurs for saturated near-surface air (see Romps 2008); for $\gamma = 1$ and T = 300K, $\mathrm{Bo}_{\mathrm{max}} = 0.32$, which suggests that the transition should occur for $\gamma \sim 0.3$. The Bowen ratio is smaller for subsaturated air: for a relative humidity of 80% and an air-sea temperature difference of 5K, Bo = 0.19. In our simulations, ΔT decreases and RH increases as γ is increased; we find that for $\gamma = 0.1$ the global-mean relative humidity and air-sea temperature difference are approximately 85% and 0.5K, giving a Bowen ratio of 0.05, consistent with the observed transition between $\gamma = 0.01$ and $\gamma = 0.1$.

The importance of the sensible heat flux in the dry regime also explains the change in the slope of the MAPE-EKE relationship at $\gamma \approx 0.2$. A large sensible heat flux implies a large air-sea temperature difference, which in turn implies stronger surface friction: Monin-Obukhov similarity theory says that the surface drag coefficient depends on the stability of the near-surface boundary layer (Troen and Mahrt 1986; Frierson et al. 2006). So as the model is moistened, the boundary layer is stabilized and surface friction weakens, causing MAPE to be converted to EKE more efficiently. We confirm this in Figure 9a, which shows the frictional contribution to the EKE budget in the GCM simulations[3]. The sink of EKE decreases exponentially with γ, partly due to slower surface winds, but also due to smaller effective drag coefficients (Figure 9b). This causes a change in the MAPE-EKE slope near $\gamma = 0.1$, although the Bowen Ratio is still <1. Changing the surface drag, for example by changing the surface roughness, could change where the transition from the dry regime to the moist regime occurs.

5. Discussion: EKE, the Entropy Budget and Atmospheric Work

Our analysis has focused on the energy budgets of the GCM simulations to explain water vapor's impact on EKE. An alternative approach to studying atmospheric EKE is to focus on the atmosphere's entropy budget or, relatedly, the work done by the atmosphere (e.g., Pauluis and Held 2002a,b; Pauluis 2007; Pauluis et al. 2008; Romps 2008; Raymond 2013; Laliberté et al. 2015). We have avoided this approach because there is ambiguity with how to define the terms in the moist GCM's entropy budget, especially those associated with artificial sources and sinks of entropy found in any numerical model, and because the entropy budget can only be used to constrain the total (zonal-mean plus eddy) kinetic energy of the atmosphere. Nevertheless, we provide here some qualitative discussion of this perspective, seeking to tie previous work to the discussion above.

The atmosphere's energy budget can be written as (Pauluis 2007; Singh and O'Neill 2022):

$$[W_{KE}] = [W_{max}] - [\Delta G], \tag{15}$$

where W_{KE} is the rate at which the atmosphere performs work to generate kinetic energy, W_{max} is the work that could be done by a dry atmosphere with the same thermal structure and ΔG is the "Gibbs penalty" required to power the hydrologic cycle. Square brackets here denote averages over

[3]The frictional contribution is calculated as a residual from the EKE budget.

appropriate spatial and temporal scales (we will not define these precisely). In the dry simulation ΔG is zero and $W_{KE} = W_{max}$, so the decrease in EKE as moisture is added reflects decreases in W_{max} and/or increases in ΔG[4].

The Gibbs penalty mostly represents the irreversible entropy production from phase changes, plus the work done to lift water (of any phase – Pauluis (2011); Singh and O'Neill (2022), though see Raymond (2013) for alternative definitions). In the case of a warming atmosphere, Laliberté et al. (2015) showed that ΔG follows Clausius-Clapeyron scaling, increasing by ~7%/K. In our simulations in which moisture is varied in isolation, we expect ΔG to have a linear contribution from increasing γ at fixed relative humidity, and an additional contribution because the free tropospheric relative humidity decreases as the GCM[5] is moistened, which leads to more entropy production from diffusion of water vapor (Pauluis 2011). Thus we expect ΔG to increase faster than linearly in γ.

W_{max} is proportional to the temperature difference between the regions where heat is put into the system and where it is extracted ($T_{in} - T_{out}$), the net radiative cooling of the atmosphere (Q_R) and the effective temperature of frictional dissipation (T_d) (Pauluis and Held 2002a; Singh and O'Neill 2022):

$$[W_{max}] = T_d Q_R \frac{T_{in} R_{out}}{(T_{in} - T_{out})^{-1}}. \tag{16}$$

The difficulty of closing the GCM's entropy budget comes in part from defining the temperatures in this equation. Nevertheless, from section 4, it is clear that $T_{in} - T_{out}$ decreases with increasing γ, both because the stability increases and because T_{in} is associated with latent heat release aloft, rather than surface sensible heating. However, the decrease in $T_{in} - T_{out}$ is opposed by an increase in Q_R, which is equal to the sum of the surface latent and sensible heat fluxes. Finally, the changes in T_d are ambiguous: decreases in surface temperatures with γ suggest T_d will decrease, but the the boundary layer also becomes shallower, which could lead to a higher effective temperature of frictional dissipation.

In summary, the thermodynamic efficiency of the GCM likely decreases rapidly (ΔG increases) as γ is increased, because the GCM can hold more water vapor and because the relative humidity

[4]Note that a dry atmosphere still has friction, so W_{max} represents the work that would be done by an ideal Carnot cycle in which the heat input and output is set by radiative cooling, surface fluxes and frictional heating.

[5]Since the evaporative flux into the atmosphere is roughly constant for all but the smallest values of γ, the partial vapor pressure in the atmosphere is also roughly fixed and the relative humidity decreases with γ

decreases. The changes in the maximum possible work done by the GCM are less clear, because there are opposing factors which could make W_{max} increase or decrease with γ. But the fact that the model's EKE decreases with increasing γ means that even if W_{max} does increase, the increases in ΔG win out.

6. Conclusion

In this study we have sought to reconcile previous work showing that moisture can both increase and decrease mid-latitude EKE. We have done this by arguing that moisture increases the growth rates of individual eddies, but makes the large-scale environment for eddy growth less favorable. For Earth-like climates, the latter effect wins out, and moisture decreases atmospheric EKE.

We have demonstrated this point using simulations with a hierarchy of idealized atmospheric models. First, we have used a moist QG model in homogeneous and channel configurations. When baroclinicity is fixed, adding moisture increases linear eddy growth rates and increases the EKE of nonlinear simulations. Both changes closely follow the scaling of Zurita-Gotor (2005), which predicts that the growth rate decreases with effective stability. In the channel configuration the baroclinicity is free to evolve, and the EKE decreases as moisture is added. In simulations with weak latent heating the EKE decreases because precipitation mostly forms on the poleward side of the jet, releasing latent heat where the model is relatively cold and decreasing the MAPE. When latent heating becomes a more important part of the model's thermodynamic budget the energetics change considerably, becoming a balance between latent heat release (which is now a source of MAPE) and radiative cooling (which is now a sink of MAPE). In this large-scale radiative-convective equilibrium, EKE production is a small residual, and saturates as the strength of the latent heating is further increased.

Next, we examined dry and moist simulations with an idealized GCM. In this model EKE also decreases as moisture is added[6], which follows changes in the MAPE. The MAPE decreases as the model is moistened because the stability increases and, to a lesser extent, because of weakened meridional temperature gradients. We have also interpreted the changes in EKE using the Lorenz Energy Cycle, focusing particularly on the diabatic terms in the MAPE budget. This reveals that, averaged over large enough scales, the mid-latitude atmosphere is roughly in radiative-convective

[6]Note that Figure 7 of O'Gorman (2011) shows that EKE increases as moisture is added to simulations with this GCM with fixed zonal-mean fields and no hydrological cycle,

equilibrium, with latent heating mostly balanced by radiative cooling. A small residual is converted to EAPE, and then to EKE. Surprisingly, these energetics are very similar to those of the strong moisture QG simulations, despite the flow in those simulations not appearing to be very Earth-like. The saturation of the EKE as moisture is added reflects the migration of atmospheric latent heat release to higher latitudes, where the atmosphere is relatively cooler. In simulations with small γ, EKE is mostly generated by surface sensible heat fluxes in the subtropics, which resembles the original description of the atmosphere's energy cycle by Lorenz (1955).

The MAPE-EKE analysis and the Lorenz Energy Cycle both suggest the presence of two regimes in the GCM. The relationship between MAPE and EKE changes slope near $\gamma = 0.2$, as MAPE is converted into EKE less efficiently in the “dry", small γ regime (i.e., the slope shallows), and we also see a transition from sensible heat fluxes driving the circulation to latent heat fluxes driving the circulation for $\gamma = 0.1$. These transitions are linked, as large sensible heat fluxes reflect large surface to near-surface air temperature gradients, implying a more unstable boundary layer and, in turn, stronger surface friction. It is this stronger surface friction which causes MAPE to be converted into EKE less efficiently in the dry regime of the GCM.

Finally, we have attempted to place our results in the context of previous work on the atmosphere's entropy budget, which has shown that moisture adds a “Gibbs penalty", which reduces the efficiency of the atmospheric heat engine. We have argued that this penalty increases faster than linear in γ because the relative humidity decreases as the model is moistened – if relative humidity were fixed we would expect the Gibbs penalty to scale linearly with γ. Changes in the maximum work done by the atmosphere, W_{max}, are harder to determine, and it is plausible that W_{max} could either increase or decrease with γ, though the decreases in EKE with γ imply that even if W_{max} increases, it does so more slowly than the Gibbs penalty.

We have thus shown that the presence of water vapor in Earth's atmosphere makes the mid-latitude circulation more sluggish, with weaker eddies and more predictable variability (Lutsko and Hell 2021). While latent heat release plays a crucial role in intensifying individual storms, these storms would be stronger in a dry atmosphere that had an environment more favorable for eddy growth. These results are very similar to studies of changes in mid-latitude EKE under warming: although a warmer atmosphere can hold more water vapor, decreases in meridional temperature gradients and increases in static stability lead to decreases in MAPE, causing reductions in EKE, as seen here (O'Gorman and Schneider 2008; Schneider et al. 2010b; O'Gorman 2010; Gertler and O'Gorman 2019). However, EKE also decreases in simulations of climates colder than that of the present-day Earth, which has been attributed to shrinking of the depth of the troposphere (O'Gorman and Schneider 2008), an effect not seen in our simulations.

To close, we discuss two implications of our results. First, the comparison of the moist QG model and the moist GCM highlights two drawbacks of moist QG models: the fixed stratification and the fact that precipitation is localized to the poleward side of the jet. The fixed stratification is a well known limitation of two-layer QG models, though they can mimic changes in "effective" stability in areas of convection (Lapeyre and Held 2003). To our knowledge, the strong localization of precipitation has not been noted before, and also presents difficulties for linking to more realistic models. In the weak moisture regime, precipitation is a sink of MAPE because it forms where the model is relatively cold, but it is always a source in the moist GCM. The bias in precipitation may also limit the usefulness of the moist QG model for other purposes. For example, the strong localized heating likely affects the position and strength of the jet, making it difficult to use the model to study jet dynamics.

A second implication of our results concerns the novel interpretation of the mid-latitudes as being in radiative-convective equilibrium (RCE) over large-scales. This provides a new way of interpreting the mid-latitude atmosphere, and emphasizes the role of latent heat release in driving the circulation. Past studies of the Lorenz Energy Cycle have often calculated the diabatic heating terms as residuals (e.g., Lembo et al. 2019), but we believe the results shown above demonstrate that these terms merit more attention. Large-scale RCE also provides a new way of interpreting past and future changes in the mid-latitude atmosphere. For example, the changes in EKE as Earth's climate is warmed or cooled described above could also be explained in terms of the distance water vapor is transported before it condenses and rains out. We intend to explore this and related questions using the large-scale RCE framework in future work.

Acknowledgments. We thank Momme Hell, Pengcheng Zhang and David Raymond for useful feedback on earlier drafts of this manuscript, and Marty Singh and Morgan O'Neill for helpful discussions about entropy budgets. We also thank the developers of the Isca climate modelling framework, which was used to run the moist GCM experiments. N.J.L. and J.M-C. were supported by the National Science Foundation through grant AGS-2202991.

Acknowledgments. We thank Momme Hell, Pengcheng Zhang and David Raymond for useful feedback on earlier drafts of this manuscript, and Marty Singh and Morgan O'Neill for helpful discussions about entropy budgets. We also thank the developers of the Isca climate modelling framework, which was used to run the moist GCM experiments. N.J.L. and J.M-C. were supported by the National Science Foundation through grant AGS-2202991.

Data availability statement. Model data and all analysis scripts will be made available upon acceptance of the manuscript

APPENDIX

A1. Potential Energy Budgets of the QG Channel Model

In the QG channel model the Mean Available Potential Energy (MAPE) and the Eddy Available Potential Energy (EAPE) are defined as:

$$\text{MAPE} \equiv [\bar{\eta}^2], \tag{A1a}$$

$$\text{EAPE} \equiv [\overline{\eta'^2}], \tag{A1b}$$

where $\eta = \Psi_1 - \Psi_2$. The MAPE and EAPE budgets are:

$$\frac{d}{dt}\text{MAPE} = C(\text{ZKE} \longrightarrow \text{MAPE}) - C(\text{MAPE} \longrightarrow \text{EAPE}) + P_z + \text{Rad}_z, \tag{A2a}$$

$$\frac{d}{dt}\text{EAPE} = C(\text{MAPE} \longrightarrow \text{EAPE}) - C(\text{EAPE} \longrightarrow \text{EKE}) + P_e + \text{Rad}_e, \tag{A2b}$$

where the conversion terms are:

$$\text{ZKE} \longrightarrow \text{MAPE} = [\bar{\eta}\partial_y(\overline{v_2}\bar{\eta})], \tag{A3a}$$

$$\text{MAPE} \longrightarrow \text{EAPE} = -[\bar{\eta}\partial_y(\overline{v_2'\eta'}])], \tag{A3b}$$

$$\text{EAPE} \longrightarrow \text{EKE} = -[\eta'\nabla\cdot\mathbf{u_2}], \tag{A3c}$$

and the precipitation and radiation terms are:

$$P_z = L[\bar{\eta}\bar{P}], \tag{A4a}$$

$$P_e = L[\overline{\eta' P'}], \tag{A4b}$$

$$\mathrm{Rad}_z = \frac{1}{\tau_d}[\bar{\eta}(\Psi_R - \bar{\eta})], \tag{A4c}$$

$$\mathrm{Rad}_e = -\frac{1}{\tau_d}[\overline{\eta'^2}]. \tag{A4d}$$

As discussed in the main text, we have calculated all terms in the potential energy budgets of the QG channel model by averaging over regions where the zonal- and time-mean potential vorticity gradients have the opposite signs in the two layers.

References

Peter R. Bannon. Linear Development of Quasi-Geostrophic Baroclinic Disturbances with Condensational Heating. *Journal of the Atmospheric Sciences*, 43(20):2261–2274, October 1986. ISSN 0022-4928, 1520-0469. doi: 10.1175/1520-0469(1986)043<2261:LDOQGB>2.0.CO;2. URL `https://journals.ametsoc.org/view/journals/atsc/43/20/1520-0469_1986_043_2261_ldoqgb_2_0_co_2.xml`. Publisher: American Meteorological Society Section: Journal of the Atmospheric Sciences.

Peter R. Bannon. Entropy Production and Climate Efficiency. *Journal of the Atmospheric Sciences*, 72(8):3268–3280, August 2015. ISSN 0022-4928, 1520-0469. doi: 10.1175/JAS-D-14-0361.1. URL `https://journals.ametsoc.org/view/journals/atsc/72/8/jas-d-14-0361.1.xml`. Publisher: American Meteorological Society Section: Journal of the Atmospheric Sciences.

Eric Bembenek, David N. Straub, and Timothy M. Merlis. Effects of Moisture in a Two-Layer Model of the Midlatitude Jet Stream. *Journal of the Atmospheric Sciences*, 77(1):131–147, 2020.

T Bischoff and T Schneider. The equatorial energy balance, itcz position, and double itcz bifurcations. *Journal of Climate*, 29(15):2997–3013, 2016.

François Bouchet, Julien Lambaerts, Guillaume Lapeyre, and Vladimir Zeitlin. Fronts and nonlinear waves in a simplified shallow-water model of the atmosphere with moisture and convection. *Physics of Fluids*, 21(11):116604, 2009. doi: 10.1063/1.3265970.

Marguerite L. Brown, Olivier Pauluis, and Edwin P. Gerber. Scaling for Saturated Moist Quasi-geostrophic Turbulence. *Journal of the Atmospheric Sciences*, 80(6):1481–1498, May 2023. ISSN 0022-4928, 1520-0469. doi: 10.1175/JAS-D-22-0215.1. URL `https://journals.ametsoc.org/view/journals/atsc/80/6/JAS-D-22-0215.1.xml`. Publisher: American Meteorological Society Section: Journal of the Atmospheric Sciences.

Junyi Chai, Malte Jansen, and Geoffrey K. Vallis. Equilibration of a Baroclinic Planetary Atmosphere toward the Limit of Vanishing Bottom Friction. *Journal of the Atmospheric Sciences*, 73(8):3249–3272, August 2016. ISSN 0022-4928, 1520-0469. doi: 10.1175/JAS-D-15-0329.1. URL `https://journals.ametsoc.org/view/journals/atsc/73/8/jas-d-15-0329.1.xml`. Publisher: American Meteorological Society Section: Journal of the Atmospheric Sciences.

Edmund K. M. Chang. An Idealized Nonlinear Model of the Northern Hemisphere Winter Storm Tracks. *Journal of the Atmospheric Sciences*, 63(7):1818–1839, July 2006. ISSN 0022-4928, 1520-0469. doi: 10.1175/JAS3726.1. URL `https://journals.ametsoc.org/view/journals/atsc/63/7/jas3726.1.xml`. Publisher: American Meteorological Society Section: Journal of the Atmospheric Sciences.

Edmund K. M. Chang, Sukyoung Lee, and Kyle L. Swanson. Storm Track Dynamics. *Journal of Climate*, 15(16):2163–2183, August 2002. ISSN 0894-8755, 1520-0442. doi: 10.1175/1520-0442(2002)015<02163:STD>2.0.CO;2. URL `https://journals.ametsoc.org/view/journals/clim/15/16/1520-0442_2002_015_02163_std_2.0.co_2.xml`. Publisher: American Meteorological Society Section: Journal of Climate.

Kerry A. Emanuel, Maurizio Fantini, and Alan J. Thorpe. Baroclinic Instability in an Environment of Small Stability to Slantwise Moist Convection. Part I: Two-Dimensional Models. *Journal of the Atmospheric Sciences*, 44(12):1559–1573, June 1987. ISSN 0022-4928, 1520-0469. doi: 10.1175/1520-0469(1987)044<1559:BIIAEO>2.0.CO;2. URL `https://journals.ametsoc.org/view/journals/atsc/44/12/1520-0469_`

1987_044_1559_biiaeo_2_0_co_2.xml. Publisher: American Meteorological Society Section: Journal of the Atmospheric Sciences.

D M W Frierson. The dynamics of idealized convection schemes and their effect on the zonally averaged tropical circulation. *Journal of the Atmospheric Sciences*, 64(23):1959–1976, 2007.

D M W Frierson, I M Held, and P Zurita-Gotor. A gray-radiation aquaplanet moist gcm. part ii: Energy transports in altered climates. *Journal of the Atmospheric Sciences*, 64(23):1680–1693, 2007.

Dargan M. W. Frierson, Isaac M. Held, and Pablo Zurita-Gotor. A Gray-Radiation Aquaplanet Moist GCM. Part I: Static Stability and Eddy Scale. *Journal of the Atmospheric Sciences*, 63 (10):2548–2566, 2006.

Charles G. Gertler and Paul A. O'Gorman. Changing available energy for extratropical cyclones and associated convection in Northern Hemisphere summer. *Proceedings of the National Academy of Sciences*, 116(10):4105–4110, March 2019. ISSN 0027-8424, 1091-6490. doi: 10.1073/pnas.1812312116. URL https://pnas.org/doi/full/10.1073/pnas.1812312116.

William J. Gutowski, Lee E. Branscome, and Douglas A. Stewart. Life Cycles of Moist Baroclinic Eddies. *Journal of the Atmospheric Sciences*, 49(4):306–319, February 1992. ISSN 0022-4928, 1520-0469. doi: 10.1175/1520-0469(1992)049<0306:LCOMBE>2.0.CO;2. URL https://journals.ametsoc.org/view/journals/atsc/49/4/1520-0469_1992_049_0306_lcombe_2_0_co_2.xml. Publisher: American Meteorological Society Section: Journal of the Atmospheric Sciences.

Dale B. Haidvogel and Isaac M. Held. Homogeneous Quasi-Geostrophic Turbulence Driven by a Uniform Temperature Gradient. *Journal of the Atmospheric Sciences*, 37(12):2644–2660, December 1980. ISSN 0022-4928, 1520-0469. doi: 10.1175/1520-0469(1980)037<2644:HQGTDB>2.0.CO;2. URL https://journals.ametsoc.org/view/journals/atsc/37/12/1520-0469_1980_037_2644_hqgtdb_2_0_co_2.xml. Publisher: American Meteorological Society Section: Journal of the Atmospheric Sciences.

I M Held and V D Larichev. A scaling theory for horizontally homogeneous, baroclinically unstable flow on a beta plane. *Journal of the Atmospheric Sciences*, 53:946–952, 1996.

Isaac M. Held and Ming Zhao. Horizontally Homogeneous Rotating Radiative–Convective Equilibria at GCM Resolution. *Journal of the Atmospheric Sciences*, 65(6):2003–2013, 2008.

J R Holton and G J Hakim. *An Introduction to Dynamic Meteorology*. Academic Press, 2013.

H. Joos and H. Wernli. Influence of microphysical processes on the potential vorticity development in a warm conveyor belt: a case-study with the limited-area model COSMO. *Quarterly Journal of the Royal Meteorological Society*, 138(663):407–418, 2012. ISSN 1477-870X. doi: 10.1002/qj.934. URL `https://onlinelibrary.wiley.com/doi/abs/10.1002/qj.934`. _eprint: https://onlinelibrary.wiley.com/doi/pdf/10.1002/qj.934.

Yeon-Hee Kim and Maeng-Ki Kim. Examination of the global lorenz energy cycle using MERRA and NCEP-reanalysis 2. *Climate Dynamics*, 40(5):1499–1513, March 2013. ISSN 1432-0894. doi: 10.1007/s00382-012-1358-4. URL `https://doi.org/10.1007/s00382-012-1358-4`.

Matthieu Kohl and Paul A. O'Gorman. The Diabatic Rossby Vortex: Growth Rate, Length Scale, and the Wave–Vortex Transition. *Journal of the Atmospheric Sciences*, 79(10):2739–2755, October 2022. ISSN 0022-4928, 1520-0469. doi: 10.1175/JAS-D-22-0022.1. URL `https://journals.ametsoc.org/view/journals/atsc/79/10/JAS-D-22-0022.1.xml`. Publisher: American Meteorological Society Section: Journal of the Atmospheric Sciences.

F. Laliberté, J. Zika, L. Mudryk, P. J. Kushner, J. Kjellsson, and K. Döös. Constrained work output of the moist atmospheric heat engine in a warming climate. *Science*, 347(6221):540–543, 2015. doi: 10.1126/science.1257103. URL `https://www.science.org/doi/abs/10.1126/science.1257103`.

J. Lambaerts, G. Lapeyre, V. Zeitlin, and F. Bouchut. Simplified two-layer models of precipitating atmosphere and their properties. *Physics of Fluids*, 23(4):046603, 2011a. doi: 10.1063/1.3582356.

Julien Lambaerts, Guillaume Lapeyre, and Vladimir Zeitlin. Moist versus Dry Barotropic Instability in a Shallow-Water Model of the Atmosphere with Moist Convection. *Journal of the Atmospheric Sciences*, 68(6):1234–1252, 2011b.

Julien Lambaerts, Guillaume Lapeyre, and Vladimir Zeitlin. Moist versus Dry Baroclinic Instability in a Simplified Two-Layer Atmospheric Model with Condensation and Latent Heat Release. *Journal of the Atmospheric Sciences*, 69(4):1405–1426, 2012.

G Lapeyre and I M Held. Diffusivity, kinetic energy dissipation, and closure theories for the poleward eddy heat flux. *Journal of the Atmospheric Sciences*, 60(23):2907–2916, 2003.

G Lapeyre and I M Held. The Role of Moisture in the Dynamics and Energetics of Turbulent Baroclinic Eddies. *Journal of the Atmospheric Sciences*, 61:1693–1710, 2004.

Alexandre Laîné, Guillaume Lapeyre, and Gwendal Rivière. A Quasigeostrophic Model for Moist Storm Tracks. *Journal of the Atmospheric Sciences*, 68(6):1306–1322, 2011.

S Lee and I M Held. Baroclinic wave packets in models and observations. *Journal of the Atmospheric Sciences*, 50:1413–1428, 1993.

Valerio Lembo, Frank Lunkeit, and Valerio Lucarini. TheDiaTo (v1.0) – a new diagnostic tool for water, energy and entropy budgets in climate models. *Geoscientific Model Development*, 12(8): 3805–3834, August 2019. ISSN 1991-959X. doi: 10.5194/gmd-12-3805-2019. URL `https://gmd.copernicus.org/articles/12/3805/2019/`. Publisher: Copernicus GmbH.

X J Levine and T Schneider. Baroclinic eddies and the extent of the hadley circulation: An idealized gcm study. *Journal of the Atmospheric Sciences*, 72(15):2744–2761, 2015.

Liming Li, Andrew P. Ingersoll, Xun Jiang, Daniel Feldman, and Yuk L. Yung. Lorenz energy cycle of the global atmosphere based on reanalysis datasets. *Geophysical Research Letters*, 34(16), 2007. ISSN 1944-8007. doi: 10.1029/2007GL029985. URL `https://onlinelibrary.wiley.com/doi/abs/10.1029/2007GL029985`. _eprint: https://onlinelibrary.wiley.com/doi/pdf/10.1029/2007GL029985.

Edward N. Lorenz. Available Potential Energy and the Maintenance of the General Circulation. *Tellus*, 7(2):157–167, 1955. ISSN 2153-3490. doi: 10.1111/j.2153-3490.1955.tb01148.x. URL `https://onlinelibrary.wiley.com/doi/abs/10.1111/j.2153-3490.1955.tb01148.x`. _eprint: https://onlinelibrary.wiley.com/doi/pdf/10.1111/j.2153-3490.1955.tb01148.x.

Edward N. Lorenz. Numerical evaluation of moist available energy. *Tellus*, 31(3):230–235, June 1979. ISSN 00402826, 21533490. doi: 10.1111/j.2153-3490.1979.tb00901.x. URL http://tellusa.net/index.php/tellusa/article/view/10429.

N J Lutsko, I M Held, and P Zurita-Gotor. Applying the fluctuation-dissipation theorem to a two-layer model of quasi-geostrophic turbulence. *Journal of the Atmospheric Sciences*, 72: 3161–3177, 2015.

Nicholas J. Lutsko and Momme C. Hell. Moisture and the Persistence of Annular Modes. *Journal of the Atmospheric Sciences*, 78(12):3951–3964, December 2021. ISSN 0022-4928, 1520-0469. doi: 10.1175/JAS-D-21-0055.1. URL https://journals.ametsoc.org/view/journals/atsc/78/12/JAS-D-21-0055.1.xml. Publisher: American Meteorological Society Section: Journal of the Atmospheric Sciences.

Nicholas J. Lutsko and Max Popp. The Influence of Meridional Gradients in Insolation and Longwave Optical Depth on the Climate of a Gray Radiation GCM. *Journal of Climate*, 31(19):7803–7822, October 2018. ISSN 0894-8755, 1520-0442. doi: 10.1175/JCLI-D-18-0103.1. URL https://journals.ametsoc.org/view/journals/clim/31/19/jcli-d-18-0103.1.xml. Publisher: American Meteorological Society Section: Journal of Climate.

Nicholas J. Lutsko, Isaac M. Held, Pablo Zurita-Gotor, and Amanda K. O'Rourke. Lower-Tropospheric Eddy Momentum Fluxes in Idealized Models and Reanalysis Data. *Journal of the Atmospheric Sciences*, 74(11):3787–3797, 2017.

Nicholas J. Lutsko, Jane Wilson Baldwin, and Timothy W. Cronin. The Impact of Large-Scale Orography on Northern Hemisphere Winter Synoptic Temperature Variability. *Journal of Climate*, 32(18):5799–5814, September 2019. ISSN 0894-8755, 1520-0442. doi: 10.1175/JCLI-D-19-0129.1. URL https://journals.ametsoc.org/view/journals/clim/32/18/jcli-d-19-0129.1.xml. Publisher: American Meteorological Society Section: Journal of Climate.

P A O'Gorman and T Schneider. The hydrological cycle over a wide range of climates simulated with an idealized gcm. *Journal of Climate*, 21(15):3815–3832, 2008a.

P A O'Gorman and T Schneider. Energy of midlatitude transient eddies in idealized simulations of changed climates. *Journal of Climate*, 21(15):5797–5806, 2008b.

Paul A. O'Gorman. Understanding the varied response of the extratropical storm tracks to climate change. *Proceedings of the National Academy of Sciences*, 107(45):19176–19180, November 2010. ISSN 0027-8424, 1091-6490. doi: 10.1073/pnas.1011547107. URL `https://pnas.org/doi/full/10.1073/pnas.1011547107`.

Paul A. O'Gorman. The Effective Static Stability Experienced by Eddies in a Moist Atmosphere. *Journal of the Atmospheric Sciences*, 68(1):75–90, January 2011. ISSN 1520-0469, 0022-4928. doi: 10.1175/2010JAS3537.1. URL `https://journals.ametsoc.org/doi/10.1175/2010JAS3537.1`.

Paul A. O'Gorman and Tapio Schneider. Energy of Midlatitude Transient Eddies in Idealized Simulations of Changed Climates. *Journal of Climate*, 21(22):5797–5806, November 2008. ISSN 0894-8755, 1520-0442. doi: 10.1175/2008JCLI2099.1. URL `https://journals.ametsoc.org/view/journals/clim/21/22/2008jcli2099.1.xml`. Publisher: American Meteorological Society Section: Journal of Climate.

Yefeng Pan, Liming Li, Xun Jiang, Gan Li, Wentao Zhang, Xinyue Wang, and Andrew P. Ingersoll. Earth's changing global atmospheric energy cycle in response to climate change. *Nature Communications*, 8(1):14367, January 2017. ISSN 2041-1723. doi: 10.1038/ncomms14367. URL `https://www.nature.com/articles/ncomms14367`. Number: 1 Publisher: Nature Publishing Group.

R. Lee Panetta. Zonal Jets in Wide Baroclinically Unstable Regions: Persistence and Scale Selection. *Journal of the Atmospheric Sciences*, 50(14):2073–2106, July 1993. ISSN 0022-4928, 1520-0469. doi: 10.1175/1520-0469(1993)050<2073:ZJIWBU>2.0.CO;2. URL `https://journals.ametsoc.org/view/journals/atsc/50/14/1520-0469_1993_050_2073_zjiwbu_2_0_co_2.xml`. Publisher: American Meteorological Society Section: Journal of the Atmospheric Sciences.

Olivier Pauluis. Sources and Sinks of Available Potential Energy in a Moist Atmosphere. *Journal of the Atmospheric Sciences*, 64(7):2627–2641, July 2007. ISSN 0022-4928, 1520-0469. doi:

10.1175/JAS3937.1. URL https://journals.ametsoc.org/view/journals/atsc/64/7/jas3937.1.xml. Publisher: American Meteorological Society Section: Journal of the Atmospheric Sciences.

Olivier Pauluis. Water Vapor and Mechanical Work: A Comparison of Carnot and Steam Cycles. *Journal of the Atmospheric Sciences*, 68(1):91–102, January 2011. ISSN 0022-4928, 1520-0469. doi: 10.1175/2010JAS3530.1. URL https://journals.ametsoc.org/view/journals/atsc/68/1/2010jas3530.1.xml. Publisher: American Meteorological Society Section: Journal of the Atmospheric Sciences.

Olivier Pauluis and Isaac M. Held. Entropy Budget of an Atmosphere in Radiative–Convective Equilibrium. Part I: Maximum Work and Frictional Dissipation. *Journal of the Atmospheric Sciences*, 59(2):125–139, January 2002a. ISSN 0022-4928, 1520-0469. doi: 10.1175/1520-0469(2002)059<0125:EBOAAI>2.0.CO;2. URL https://journals.ametsoc.org/view/journals/atsc/59/2/1520-0469_2002_059_0125_eboaai_2.0.co_2.xml. Publisher: American Meteorological Society Section: Journal of the Atmospheric Sciences.

Olivier Pauluis and Isaac M. Held. Entropy Budget of an Atmosphere in Radiative–Convective Equilibrium. Part II: Latent Heat Transport and Moist Processes. *Journal of the Atmospheric Sciences*, 59(2):140–149, January 2002b. ISSN 0022-4928, 1520-0469. doi: 10.1175/1520-0469(2002)059<0140:EBOAAI>2.0.CO;2. URL https://journals.ametsoc.org/view/journals/atsc/59/2/1520-0469_2002_059_0140_eboaai_2.0.co_2.xml. Publisher: American Meteorological Society Section: Journal of the Atmospheric Sciences.

Olivier Pauluis, Arnaud Czaja, and Robert Korty. The global atmospheric circulation on moist isentropes. *Science*, 321(5892):1075–1078, 2008. doi: 10.1126/science.1159649. URL https://www.science.org/doi/abs/10.1126/science.1159649.

V Pavan and I M Held. The diffusive approximation for eddy fluxes in baroclinically unstable jets. *Journal of the Atmospheric Sciences*, 53:1262–1272, 1996.

T Pierrehumbert, H Brogniez, and R Roca. On the relative humidity of the atmosphere. In T Schneider and A Sobel, editors, *The Global Circulation of the Atmosphere*, chapter 6, pages 143–185. Princeton University Press, Princeton, 2007.

David J. Raymond. Sources and sinks of entropy in the atmosphere. *Journal of Advances in Modeling Earth Systems*, 5(4):755–763, 2013. ISSN 1942-2466. doi: 10.1002/jame.20050. URL `https://onlinelibrary.wiley.com/doi/abs/10.1002/jame.20050`. _eprint: https://onlinelibrary.wiley.com/doi/pdf/10.1002/jame.20050.

Richard J. Reed, Mark D. Albright, Adrian J. Sammons, and Per Undén. The Role of Latent Heat Release in Explosive Cyclogenesis: Three Examples Based on ECMWF Operational Forecasts. *Weather and Forecasting*, 3(3):217–229, September 1988. ISSN 1520-0434, 0882-8156. doi: 10.1175/1520-0434(1988)003<0217:TROLHR>2.0.CO;2. URL `https://journals.ametsoc.org/view/journals/wefo/3/3/1520-0434_1988_003_0217_trolhr_2_0_co_2.xml`. Publisher: American Meteorological Society Section: Weather and Forecasting.

Joy Romanski and William B. Rossow. Contributions of Individual Atmospheric Diabatic Heating Processes to the Generation of Available Potential Energy. *Journal of Climate*, 26(12):4244–4263, June 2013. ISSN 0894-8755, 1520-0442. doi: 10.1175/JCLI-D-12-00457.1. URL `https://journals.ametsoc.org/view/journals/clim/26/12/jcli-d-12-00457.1.xml`. Publisher: American Meteorological Society Section: Journal of Climate.

David M. Romps. The Dry-Entropy Budget of a Moist Atmosphere. *Journal of the Atmospheric Sciences*, 65(12):3779–3799, December 2008. ISSN 0022-4928, 1520-0469. doi: 10.1175/2008JAS2679.1. URL `https://journals.ametsoc.org/view/journals/atsc/65/12/2008jas2679.1.xml`. Publisher: American Meteorological Society Section: Journal of the Atmospheric Sciences.

Tapio Schneider and Paul A. O'Gorman. Moist Convection and the Thermal Stratification of the Extratropical Troposphere. *Journal of the Atmospheric Sciences*, 65(11):3571–3583, November 2008. ISSN 1520-0469, 0022-4928. doi: 10.1175/2008JAS2652.1. URL `https://journals.ametsoc.org/doi/10.1175/2008JAS2652.1`.

Tapio Schneider and Christopher C. Walker. Self-Organization of Atmospheric Macroturbulence into Critical States of Weak Nonlinear Eddy–Eddy Interactions. *Journal of the Atmospheric*

Sciences, 63(6):1569–1586, June 2006. ISSN 1520-0469, 0022-4928. doi: 10.1175/JAS3699.1. URL https://journals.ametsoc.org/doi/10.1175/JAS3699.1.

Tapio Schneider and Christopher C. Walker. Scaling Laws and Regime Transitions of Macro-turbulence in Dry Atmospheres. *Journal of the Atmospheric Sciences*, 65(7):2153–2173, July 2008. ISSN 1520-0469, 0022-4928. doi: 10.1175/2007JAS2616.1. URL https://journals.ametsoc.org/doi/10.1175/2007JAS2616.1.

Tapio Schneider, Paul A. O'Gorman, and Xavier J. Levine. Water vapor and the dynamics of climate changes. *Reviews of Geophysics*, 48(3), 2010a.

Tapio Schneider, Paul A. O'Gorman, and Xavier J. Levine. WATER VAPOR AND THE DYNAMICS OF CLIMATE CHANGES. *Reviews of Geophysics*, 48(3):RG3001, July 2010b. ISSN 8755-1209. doi: 10.1029/2009RG000302. URL http://doi.wiley.com/10.1029/2009RG000302.

S. C. Sherwood, R. Roca, T. M. Weckwerth, and N. G. Andronova. Tropospheric water vapor, convection, and climate. *Reviews of Geophysics*, 48(2):RG2001, April 2010. ISSN 8755-1209. doi: 10.1029/2009RG000301. URL http://doi.wiley.com/10.1029/2009RG000301.

Martin S. Singh and Morgan E O'Neill. The climate system and the second law of thermodynamics. *Rev. Mod. Phys.*, 94:015001, Jan 2022. doi: 10.1103/RevModPhys.94.015001. URL https://link.aps.org/doi/10.1103/RevModPhys.94.015001.

I. B. Troen and L. Mahrt. A simple model of the atmospheric boundary layer; sensitivity to surface evaporation. *Boundary-Layer Meteorology*, 37(1):129–148, October 1986. ISSN 1573-1472. doi: 10.1007/BF00122760. URL https://doi.org/10.1007/BF00122760.

Heini Wernli, Sebastien Dirren, Mark A. Liniger, and Matthias Zillig. Dynamical aspects of the life cycle of the winter storm 'Lothar' (24–26 December 1999). *Quarterly Journal of the Royal Meteorological Society*, 128 (580):405–429, 2002. ISSN 1477-870X. doi: 10.1256/003590002321042036. URL https://onlinelibrary.wiley.com/doi/abs/10.1256/003590002321042036. _eprint: https://onlinelibrary.wiley.com/doi/pdf/10.1256/003590002321042036.

Robert C. J. Wills and Tapio Schneider. Mechanisms Setting the Strength of Orographic Rossby Waves across a Wide Range of Climates in a Moist Idealized GCM. *Journal of Climate*, 31(18):7679–7700, September 2018. ISSN 0894-8755, 1520-0442. doi: 10.1175/JCLI-D-17-0700.1. URL `https://journals.ametsoc.org/view/journals/clim/31/18/jcli-d-17-0700.1.xml`. Publisher: American Meteorological Society Section: Journal of Climate.

Wenyu Zhou, Isaac M. Held, and Stephen T. Garner. Tropical Cyclones in Rotating Radiative–Convective Equilibrium with Coupled SST. *Journal of the Atmospheric Sciences*, 74(3): 879–892, 2017.

P Zurita-Gotor. On the sensitivity of zonal-index persistence to friction. *Journal of the Atmospheric Sciences*, 71:3788–3800, 2014.

P Zurita-Gotor, J Blanco-Fuentes, and E P Gerber. The impact of baroclinic eddy feedback on the persistence of jet variability in the two-layer model. *Journal of the Atmospheric Sciences*, 71: 410–429, 2014.

Pablo Zurita-Gotor. Updraft/Downdraft Constraints for Moist Baroclinic Modes and Their Implications for the Short-Wave Cutoff and Maximum Growth Rate. *Journal of the Atmospheric Sciences*, 62(12):4450–4458, December 2005. ISSN 0022-4928, 1520-0469. doi: 10.1175/JAS3630.1. URL `https://journals.ametsoc.org/view/journals/atsc/62/12/jas3630.1.xml`. Publisher: American Meteorological Society Section: Journal of the Atmospheric Sciences.